Levan, A, Gompertz, BP, Salafia, OS, Bulla, M, Burns, E, Hotokezaka, K, Izzo, L, Lamb, GP, Malesani, DB, Oates, SR, Ravasio, ME, Rouco Escorial, A, Schneider, B, Sarin, N, Schulze, S, Tanvir, NR, Ackley, K, Anderson, G, Brammer, GB, Christensen, L, Dhillon, VS, Evans, PA, Fausnaugh, M, Fong, W-F, Fruchter, AS, Fryer, C, Fynbo, JPU, Gaspari, N, Heintz, KE, Hjorth, J, Kennea, JA, Kennedy, MR, Laskar, T, Leloudas, G, Mandel, I, Martin-Carrillo, A, Metzger, BD, Nicholl, M, Nugent, A, Palmerio, JT, Pugliese, G, Rastinejad, J, Rhodes, L, Rossi, A, Saccardi, A, Smartt, SJ, Stevance, HF, Tohuvavohu, A, van der Horst, A, Vergani, SD, Watson, D, Barclay, T, Bhirombhakdi, K, Breedt, E, Breeveld, AA, Brown, AJ, Campana, S, Chrimes, AA, D'Avanzo, P, D'Elia, V, De Pasquale, M, Dyer, MJ, Galloway, DK, Garbutt, JA, Green, MJ, Hartmann, DH, Jakobsson, P, Kerry, P, Kouveliotou, C, Langeroodi, D, Le Floc'h, E, Leung, JK, Littlefair, SP, Munday, J, O'Brien, P, Parsons, SG, Pelisoli, I, Sahman, DI, Salvaterra, R, Sbarufatti, B, Steeghs, D, Tagliaferri, G, Thöne, CC, de Ugarte Postigo, A and Kann, DA

Heavy element production in a compact object merger observed by JWST

Article

Heavy element production in a compact object merger observed by JWST

Andrew Levan[1,2*], Benjamin P. Gompertz[3], Om Sharan Salafia[4,5], Mattia Bulla[6,7,8], Eric Burns[9], Kenta Hotokezaka[10,11], Luca Izzo[12,13], Gavin P. Lamb[14,15], Daniele B. Malesani[1,16,17], Samantha R. Oates[3], Maria Edvige Ravasio[1,4], Alicia Rouco Escorial[18], Benjamin Schneider[19], Nikhil Sarin[20,21], Steve Schulze[21], Nial R. Tanvir[15], Kendall Ackley[2], Gemma Anderson[22], Gabriel B. Brammer[16,17], Lise Christensen[16,17], Vikram S. Dhillon[23,24], Phil A. Evans[15], Michael Fausnaugh[19,25], Wen-fai Fong[26,27], Andrew S. Fruchter[28], Chris Fryer[29,30,31,32], Johan P. U. Fynbo[16,17], Nicola Gaspari[1], Kasper E. Heintz[16,17], Jens Hjorth[12], Jamie A. Kennea[33], Mark R. Kennedy[34,35], Tanmoy Laskar[1,36], Giorgos Leloudas[37], Ilya Mandel[38,39], Antonio Martin-Carrillo[40], Brian D. Metzger[41,42], Matt Nicholl[43], Anya Nugent[26,27], Jesse T. Palmerio[44], Giovanna Pugliese[45], Jillian Rastinejad[26,27], Lauren Rhodes[46], Andrea Rossi[47], Andrea Saccardi[44], Stephen J. Smartt[43,46], Heloise F. Stevance[46,48], Aaron Tohuvavohu[49], Alexander van der Horst[32], Susanna D. Vergani[44], Darach Watson[16,17], Thomas Barclay[50], Kornpob Bhirombhakdi[28], Elmé Breedt[51], Alice A. Breeveld[52], Alexander J. Brown[23], Sergio Campana[4], Ashley A. Chrimes[1], Paolo D'Avanzo[4], Valerio D'Elia[53,54], Massimiliano De Pasquale[55], Martin J. Dyer[23], Duncan K. Galloway[38,39], James A. Garbutt[23], Matthew J. Green[56], Dieter H. Hartmann[57], Páll Jakobsson[58], Paul Kerry[23], Chryssa Kouveliotou[32], Danial Langeroodi[12], Emeric Le Floc'h[59], James K. Leung[60,61,39], Stuart P. Littlefair[23], James Munday[2,62], Paul O'Brien[15], Steven G. Parsons[23], Ingrid Pelisoli[2], David I. Sahman[23], Ruben Salvaterra[63], Boris Sbarufatti[4], Danny Steeghs[2,39], Gianpiero Tagliaferri[4],

Christina C. Thöne[64], Antonio de Ugarte Postigo[65], David Alexander Kann[66]

[1]Department of Astrophysics/IMAPP, Radboud University, 6525 AJ Nijmegen, The Netherlands.
[2]Department of Physics, University of Warwick, Coventry, CV4 7AL, UK.
[3]Institute for Gravitational Wave Astronomy and School of Physics and Astronomy, University of Birmingham, Birmingham, B15 2TT, UK.
[4]INAF - Osservatorio Astronomico di Brera, Via E. Bianchi 46, I-23807, Merate (LC), Italy.
[5]INFN - Sezione di Milano-Bicocca, Piazza della Scienza 2, I-20146, Milano (MI), Italy.
[6]Department of Physics and Earth Science, University of Ferrara, via Saragat 1, I-44122 Ferrara, Italy.
[7]INFN, Sezione di Ferrara, via Saragat 1, I-44122 Ferrara, Italy.
[8]INAF, Osservatorio Astronomico dAbruzzo, via Mentore Maggini snc, 64100 Teramo, Italy.
[9]Department of Physics & Astronomy, Louisiana State University, Baton Rouge, LA 70803, USA.
[10]Research Center for the Early Universe, Graduate School of Science, The University of Tokyo, Bunkyo, Tokyo 113-0033, Japan.
[11]Kavli IPMU (WPI), UTIAS, The University of Tokyo, Kashiwa, Chiba 277-8583, Japan.
[12]DARK, Niels Bohr Institute, University of Copenhagen, Jagtvej 128, 2200 Copenhagen N, Denmark.
[13]INAF-Osservatorio Astronomico di Capodimonte, Salita Moiariello 16, 80131, Napoli, Italy.
[14]Astrophysics Research Institute, Liverpool John Moores University, IC2 Liverpool Science Park, Liverpool, L3 5RF, Liverpool, UK.
[15]School of Physics & Astronomy, University of Leicester, University Road, Leicester, LE1 7RH, UK.
[16]Cosmic Dawn Center (DAWN), Denmark.
[17]Niels Bohr Institute, University of Copenhagen, Jagtvej 128, 2200 Copenhagen N, Denmark.
[18]European Space Agency (ESA), European Space Astronomy Centre (ESAC), Camino Bajo del Castillo s/n, 28692 Villanueva de la Caada, Madrid, Spain.
[19]Kavli Institute for Astrophysics and Space Research, Massachusetts Institute of Technology, 77 Massachusetts Ave, Cambridge, MA 02139, USA.

[20]Nordita, Stockholm University and KTH Royal Institute of Technology Hannes Alfvns vg 12, SE-106 91 Stockholm, Sweden.
[21]The Oskar Klein Centre, Department of Physics, Stockholm University, AlbaNova, SE-106 91 Stockholm, Sweden.
[22]International Centre for Radio Astronomy Research, Curtin University, GPO Box U1987, Perth, WA 6845, Australia.
[23]Department of Physics and Astronomy, University of Sheffield, Sheffield, S3 7RH, United Kingdom.
[24]Instituto de Astrofísica de Canarias, E-38205 La Laguna, Tenerife, Spain.
[25]Department of Physics & Astronomy, Texas Tech University, Lubbock TX, 79410-1051, USA.
[26]Center for Interdisciplinary Exploration and Research in Astrophysics, Northwestern University, 1800 Sherman Ave., Evanston, 60208, IL, USA.
[27]Department of Physics and Astronomy, Northwestern University, 2145 Sheridan Road, Evanston, 60208-3112, IL, USA.
[28]Space Telescope Science Institute, 3700 San Martin Drive, Baltimore, MD 21218.
[29]Center for Theoretical Astrophysics, Los Alamos National Laboratory, Los Alamos, NM 87545.
[30]Department of Astronomy, The University of Arizona, Tucson, AZ 85721.
[31]Department of Physics and Astronomy, The University of New Mexico, Albuquerque, NM 87131.
[32]Department of Physics, The George Washington University, Washington, DC 20052.
[33]Department of Astronomy and Astrophysics, The Pennsylvania State University, 525 Davey Lab, University Park, PA 16802, USA.
[34]School of Physics, Kane Building, University College Cork, Cork, Ireland.
[35]Jodrell Bank Centre for Astrophysics, Department of Physics and Astronomy, The University of Manchester, M13 9PL, UK.
[36]Department of Physics & Astronomy, University of Utah, Salt Lake City, UT 84112, USA.
[37]DTU Space, National Space Institute, Technical University of Denmark, Elektrovej 327, 2800 Kgs. Lyngby, Denmark.
[38]School of Physics and Astronomy, Monash University, Clayton, Victoria 3800, Australia.
[39]ARC Center of Excellence for Gravitational Wave Discovery – OzGrav.

[40]School of Physics and Centre for Space Research, University College Dublin, Belfield, Dublin 4, Ireland.
[41]Department of Physics and Columbia Astrophysics Laboratory, Columbia University, New York, NY 10027, USA.
[42]Center for Computational Astrophysics, Flatiron Institute, 162 5th Ave, New York, NY 10010, USA.
[43]Astrophysics Research Centre, School of Mathematics and Physics, Queens University Belfast, Belfast BT7 1NN, UK.
[44]GEPI, Observatoire de Paris, Universit PSL, CNRS, 5 Place Jule Janssen, 92190 Meudon, France.
[45]Astronomical Institute Anton Pannekoek, University of Amsterdam, 1090 GE Amsterdam, The Netherlands.
[46]Department of Physics, University of Oxford, Keble Road, Oxford, OX1 3RH, UK.
[47]INAF-Osservatorio di Astrofisica e Scienza dello Spazio, Via Piero Gobetti 93/3, 40129 Bologna, Italy.
[48]Department of Physics, The University of Auckland, Private Bag 92019, Auckland, New Zealand.
[49]Department of Astronomy & Astrophysics, University of Toronto, Toronto, ON M5S 3H4.
[50]NASA Goddard Space Flight Center, 8800 Greenbelt Road, Greenbelt, MD 20771, USA.
[51]Institute of Astronomy, University of Cambridge, Madingley Road, Cambridge CB3 0HA, UK.
[52]University College London, Mullard Space Science Laboratory, Holmbury St. Mary, Dorking, RH5 6NT, UK.
[53]ASI/SSDC, Via del Politecnico SNC, I-00133, Rome, Italy.
[54]INAF/OAR, Via Frascati 33, I-00040, Monteporzio Catone, Rome, Italy.
[55]University of Messina, Polo Papardo, Department of Mathematics, Physics, Informatics and Earth Sciences, via F.S. D'Alcontres 31, 98166 Messina, Italy.
[56]School of Physics and Astronomy, Tel-Aviv University, Tel-Aviv 6997801, Israel.
[57]Department of Physics and Astronomy & Clemson University, Clemson, SC 29634-0978.
[58]Centre for Astrophysics and Cosmology, Science Institute, University of Iceland, Dunhagi 5, 107 Reykjavik, Iceland.
[59]CEA, IRFU, DAp, AIM, Universit Paris-Saclay, Universit Paris Cit, Sorbonne Paris Cit, CNRS, F-91191 Gif-sur-Yvette, France.

[60]Sydney Institute for Astronomy, School of Physics, The University of Sydney, NSW 2006, Australia.
[61]CSIRO Space and Astronomy, PO Box 76, Epping, NSW 1710, Australia.
[62]Isaac Newton Group of Telescopes, Apartado de Correos 368, E-38700 Santa Cruz de La Palma, Spain.
[63]INAF/IASF-MI, Via Alfonso Corti 12, I-20133, Milano, Italy.
[64]Astronomical Institute of the Czech Academy of Sciences, Fričova 298, 251 65 Ondřejov, Czech Republic.
[65]Artemis, Observatoire de la Côte d'Azur, Université Cte d'Azur, Boulevard de l'Observatoire, F-06304 Nice, France.
[66]Hessian Research Cluster ELEMENTS, Giersch Science Center, Max-von-Laue-Straße 12, Goethe University Frankfurt, Campus Riedberg, D-60438 Frankfurt am Main, Germany.

*Corresponding author(s). E-mail(s): a.levan@astro.ru.nl;

Abstract

The mergers of binary compact objects such as neutron stars and black holes are of central interest to several areas of astrophysics, including as the progenitors of gamma-ray bursts (GRBs) [1], sources of high-frequency gravitational waves (GW)[2] and likely production sites for heavy element nucleosynthesis via rapid neutron capture (the ***r***-process) [3]. Here we present observations of the exceptionally bright gamma-ray burst GRB 230307A. We show that GRB 230307A belongs to the class of long-duration gamma-ray bursts associated with compact object mergers[4, 5, 6], and contains a kilonova similar to AT2017gfo, associated with the gravitational-wave merger GW170817 [7, 8, 9, 10, 11, 12]. We obtained James Webb Space Telescope mid-infrared (mid-IR) imaging and spectroscopy 29 and 61 days after the burst. The spectroscopy shows an emission line at 2.15 microns which we interpret as tellurium (atomic mass A=130), and a very red source, emitting most of its light in the mid-IR due to the production of lanthanides. These observations demonstrate that nucleosynthesis in GRBs can create ***r***-process elements across a broad atomic mass range and play a central role in heavy element nucleosynthesis across the Universe.

GRB 230307A was detected by the *Fermi* Gamma-ray Burst Monitor (GBM) and GECAM at 15:44:06 UT on 7 Mar 2023 [13, 14]. Its measured duration of $T_{90} \sim 35$ s and exceptionally high prompt fluence of $(2.951 \pm 0.004) \times 10^{-3}\,\mathrm{erg\,cm^{-2}}$ in the 10-1000 keV band make it the second-brightest GRB ever detected, and ostensibly a "long-soft" GRB (Figure 1).

The burst was also detected by several other high-energy instruments (Methods), enabling source triangulation by the InterPlanetary Network (IPN). The *Neil Gehrels Swift Observatory* (*Swift*) tiled the IPN localisation [15] which revealed one candidate X-ray afterglow [16]. We obtained optical observations of the field with the ULTRACAM instrument, mounted on the 3.5m New Technology Telescope (NTT). These observations revealed a new source coincident with the *Swift* X-ray source, and we identified it as the optical afterglow of GRB 230307A [17]. Given the very bright prompt emission, the afterglow is unusually weak (Figure 1).

We obtained extensive follow-up observations in the optical and near-infrared with the Gemini South Telescope and the Very Large Telescope (VLT); in the X-ray with the *Swift*/XRT and the Chandra X-ray observatory; and in the radio with the Australia Telescope Compact Array (ATCA) and MeerKAT. Multi Unit Spectroscopic Explorer (MUSE) integral field spectrograph observations provided the redshift of a bright spiral galaxy at $z = 0.0646 \pm 0.0001$ offset 30.2 arcseconds (38.9 kiloparsec in projection) from the burst position (Figure 2, also [18]).

Our ground-based campaign spans 1.4 to 41 days after the burst (Extended Data Table 1 and 2). At 11 days, infrared observations demonstrated a transition from an early blue spectral slope, to a much redder one, consistent with the appearance of a kilonova [19, 3]. Based on this detection, we requested James Webb Space Telescope (JWST) observations, which were initiated on 5 April 2023. At the first epoch (+28.9 days after GRB), we took 6-colour observations with the Near Infrared Camera (NIRCam) (Figure 2), as well as a spectrum with the Near Infrared Spectrograph (NIRSpec) covering $0.5 - 5.5$ microns (Figure 3).

The NIRCam observations reveal an extremely red source with F150W(AB) $= 28.11 \pm 0.12$ mag and F444W(AB) $= 24.4 \pm 0.01$ mag. A faint galaxy is detected in these data with NIRSpec providing a redshift of $z = 3.87$, offset approximately 0.3 arcseconds from the burst position. The probability of chance alignment for this galaxy, and the $z = 0.065$ spiral are comparable. However, the burst's properties are inconsistent with an origin at $z = 3.87$; the implied isotropic equivalent energy release would exceed all known GRBs by an order of magnitude or more, the luminosity and colour evolution of the counterpart would be unlike any observed GRB afterglow or supernova (Supplementary Information). A second epoch of JWST observations was obtained approximately 61 days after the burst. These observations showed that the source had faded by 2.4 magnitudes in F444W, demonstrating a rapid decay expected in a low redshift the kilonova scenario and effectively ruling out alternatives (Supplementary Information). We therefore conclude that GRB 230307A originated from the galaxy at $z = 0.065$.

Some properties of GRB 230307A are remarkably similar to those of the bright GRB 211211A, which was also accompanied by a kilonova [4, 5, 6]. In particular, the prompt emission consists of a hard pulse lasting for ~ 19 seconds, followed by much softer emission. The prompt emission spectrum is well modelled by a double broken power-law with two spectral breaks moving through the gamma-ray band (Methods), suggesting a synchrotron origin of the emission [20]. The X-ray afterglow is exceptionally faint, much fainter than most bursts when scaled by the prompt GRB fluence (see Figure 1and Supplementary Information). The development of the optical and IR

counterpart is also similar to GRB 211211A, with an early blue colour and a subsequent transition to red on a timescale of a few days. In Figure 4, we plot the evolution of the counterpart compared with the kilonova AT2017gfo [7, 8, 9, 10, 11, 12, 21, 22], identified in association with the gravitational-wave detected binary neutron star merger, GW170817 [2]. AT2017gfo is the most rapidly evolving thermal transient ever observed; much more rapid than supernovae or even fast blue optical transients [23]. The counterpart of GRB 230307A appears to show near identical decline rates to AT2017gfo both at early times in the optical and IR, and later in the mid-IR [24]. These similarities are confirmed by a joint fit of afterglow and kilonova models to our multi-wavelength data (Supplementary Information).

The JWST observations provide a detailed view of kilonova evolution. On timescales of ~ 30 days, it is apparent that the kilonova emits almost all of its light in the mid-infrared, beyond the limits of sensitive ground-based observations. This is consistent with some previous model predictions [25]. Strikingly, despite its powerful and long-lived prompt emission that starkly contrasts GW170817/GRB 170817A, the GRB 230307A kilonova is remarkably similar to AT 2017gfo. This was also the case for GRB 211211A [4, 5, 6, 26], and suggests the kilonova signal is relatively insensitive to the GRB.

Our NIRSpec spectrum shows a broad emission feature with a central wavelength of 2.15 microns, visible in both epochs of JWST spectroscopy (Figure 3). At longer wavelengths, the spectrum displays a slowly rising continuum up to 4.5 microns followed by either an additional feature or change of spectral slope. The colours of the counterpart at this time can be explained by kilonova models (Supplementary Information).

A similar emission-like feature is also visible in the later epochs of X-shooter observations of AT2017gfo [9], measured at 2.1 microns by [27]. Furthermore, the later time mid-IR emission and colours are consistent with those observed with AT2017gfo with *Spitzer* [24]. These similarities further strengthen both the kilonova interpretation and the redshift measurement of GRB 230307A (Figure 3). We interpret this feature as arising from the forbidden [Te III] transition between the ground level and the first fine structure level of tellurium, with an experimentally determined wavelength of 2.1019 microns [28]. The presence of tellurium is plausible, as it lies at the second peak in the r-process abundance pattern, which occurs at atomic masses around $A \approx 130$ [29]. Therefore, it should be abundantly produced in kilonovae, as seen in hydrodynamical simulations of binary neutron star mergers with nucleosynthetic compositions similar to those favoured for AT2017gfo [30]. Furthermore, the typical ionisation state of Te in kilonova ejecta is expected to be Te III at this epoch because of the efficient radioactive ionisation [31]. Tellurium has recently been suggested as the origin of the same feature in the spectrum of AT2017gfo [32]. A previous study [27] also identified this tellurium transition and noted that the observed feature is most likely two blended emission lines. Tellurium can also be produced via the slower capture of neutrons in the s-process. Indeed, this line is also seen in planetary nebulae [33]. The detection of [Te III] 2.1 μm provides an additional r-process element, building on the earlier detection of strontium [34]. Importantly, while strontium is a light r-process element associated with the so-called first peak, tellurium is a heavier second-peak element, requiring different nucleosynthetic pathways. The mass of Te III estimated from the

observed line flux is $\sim 10^{-3} M_\odot$ (Supplementary Information). Although weaker, we also note that the spectral feature visible at 4.5 microns is approximately consistent with the expected location of the first peak element selenium and the near-third peak element tungsten [35]. In future events, further elemental lines can be used to resolve this difference [35], with very different appearances redward of the NIRSpec cut-off (5.5 microns). For nearby kilonovae, observations should also be plausible by JWST with MIRI out to 15 microns.

Detailed spectral fitting at late epochs is challenging because of the breakdown of the assumptions regarding local thermodynamic equilibrium (LTE) which are used to predict kilonova spectra at earlier ages, as well as fundamental uncertainties in the atomic physics of r-process elements. However, these observations provide a calibration sample for informing future models. The red continuum emission indicates large opacity in the mid-IR at low temperatures, e.g., $\sim 10\,\mathrm{cm^2 g^{-1}}$ at $\sim 700\,\mathrm{K}$, which may suggest that lanthanides(atomic numbers 58-71) are abundant in the ejecta.

The host galaxy is a low mass system ($\sim 2.5 \times 10^9\ M_\odot$) dominated by an old population. The large offset is consistent with the largest offsets seen in short GRBs [36, 37] and could be attained by a binary with a velocity of a few hundred km $\mathrm{s^{-1}}$ and a merger time $> 10^8$ years. Alternatively, the faint optical/IR detection of the source at the second JWST observation could be due to an underlying globular cluster host which could create compact object systems at enhanced rates via dynamical interactions [38].

It is striking that GRB 230307A is an extremely bright GRB, with only the exceptional GRB 221009A being brighter [39]. The detection of kilonovae in two of the ten most fluent *Fermi*/GBM GRBs implies that mergers may contribute significantly to the bright GRB population (see Supplementary Information). Indeed, several further long GRBs including GRB 060614 [40, 41], GRB 111005A [42] and GRB 191019A [43] have been suggested to arise from mergers. If a substantial number of long GRBs are associated with compact object mergers, they provide an essential complement to gravitational-wave detections. Firstly, joint GW-GRB detections, including long GRBs, can push the effective horizons of GW detectors to greater distances and provide much smaller localisations [4, 44]. Secondly, long GRBs can be detected without GW detectors, providing a valuable route for enhancing kilonova detections. Thirdly, JWST can detect kilonova emission at redshifts substantially beyond the horizons of the current generation of GW detectors, enabling the study of kilonovae across a greater volume of the Universe.

The duration of the prompt γ-ray emission in these mergers remains challenging to explain. In particular, the natural timescales for emission in compact object mergers are much shorter than the measured duration of GRB 230307A. Previously suggested models that may also explain GRB 230307A include magnetars [45], black hole - neutron star mergers [46, 47], or even neutron star - white dwarf systems [6]. It has also been suggested that collapsars may power the r-process [48], in which case one may interpret GRB 230307A as an unusual collapsar. However, such a progenitor is not plausible since there is no star formation at the location of GRB 230307A. The duration problem might become immaterial if the jet timescale does not directly track the accretion timescale in the post-merger system. Such a behaviour has been

recently proposed based on insights from general-relativistic magneto-hydrodynamical simulations [49, 50], which suggest that the duration of the jet can extend up to several times the disk viscous timescale, creating long GRBs from short-lived mergers.

References

[1] Tanvir, N. R. *et al.* A 'kilonova' associated with the short-duration γ-ray burst GRB 130603B. *Nature* **500**, 547–549 (2013).

[2] Abbott, B. P., Abbott, R., Abbott, T. D. *et al.* GW170817: Observation of Gravitational Waves from a Binary Neutron Star Inspiral. *Phys. Rev. Lett.* **119**, 161101 (2017).

[3] Metzger, B. D. Kilonovae. *Living Reviews in Relativity* **23**, 1 (2019).

[4] Rastinejad, J. C. *et al.* A kilonova following a long-duration gamma-ray burst at 350 Mpc. *Nature* **612**, 223–227 (2022).

[5] Troja, E. *et al.* A nearby long gamma-ray burst from a merger of compact objects. *Nature* **612**, 228–231 (2022).

[6] Yang, J. *et al.* A long-duration gamma-ray burst with a peculiar origin. *Nature* **612**, 232–235 (2022).

[7] Arcavi, I. *et al.* Optical emission from a kilonova following a gravitational-wave-detected neutron-star merger. *Nature* **551**, 64–66 (2017).

[8] Coulter, D. A. *et al.* Swope Supernova Survey 2017a (SSS17a), the optical counterpart to a gravitational wave source. *Science* **358**, 1556–1558 (2017).

[9] Pian, E. *et al.* Spectroscopic identification of r-process nucleosynthesis in a double neutron-star merger. *Nature* **551**, 67–70 (2017).

[10] Smartt, S. J. *et al.* A kilonova as the electromagnetic counterpart to a gravitational-wave source. *Nature* **551**, 75–79 (2017).

[11] Tanvir, N. R. *et al.* The Emergence of a Lanthanide-rich Kilonova Following the Merger of Two Neutron Stars. *Astrophys. J. Lett.* **848**, L27 (2017).

[12] Soares-Santos, M. *et al.* The Electromagnetic Counterpart of the Binary Neutron Star Merger LIGO/Virgo GW170817. I. Discovery of the Optical Counterpart Using the Dark Energy Camera. *Astrophys. J. Lett.* **848**, L16 (2017).

[13] Fermi GBM Team. GRB 230307A: Fermi GBM Final Real-time Localization. *GRB Coordinates Network* **33405**, 1 (2023).

[14] Xiong, S., Wang, C., Huang, Y. & Gecam Team. GRB 230307A: GECAM detection of an extremely bright burst. *GRB Coordinates Network* **33406**, 1 (2023).

[15] Kozyrev, A. S. *et al.* Further improved IPN localization for GRB 230307A. *GRB Coordinates Network* **33461**, 1 (2023).

[16] Burrows, D. N. *et al.* GRB 230307A: Swift-XRT observations. *GRB Coordinates Network* **33429**, 1 (2023).

[17] Levan, A. J., Gompertz, B., Ackley, K., Kennedy, M. & Dhillon, V. GRB 230307A: Possible optical afterglow. *GRB Coordinates Network* **33439**, 1 (2023).

[18] Gillanders, J., O'Connor, B., Dichiara, S. & Troja, E. GRB 230307A: Continued Gemini-South observations confirm rapid optical fading. *GRB Coordinates Network* **33485**, 1 (2023).

[19] Li, L.-X. & Paczyński, B. Transient Events from Neutron Star Mergers. *Astrophys. J. Lett.* **507**, L59–L62 (1998).
[20] Gompertz, B. P. *et al.* The case for a minute-long merger-driven gamma-ray burst from fast-cooling synchrotron emission. *Nature Astronomy* **7**, 67–79 (2023).
[21] Valenti, S. *et al.* The Discovery of the Electromagnetic Counterpart of GW170817: Kilonova AT 2017gfo/DLT17ck. *Astrophys. J. Lett.* **848**, L24 (2017).
[22] Villar, V. A. *et al.* The Combined Ultraviolet, Optical, and Near-infrared Light Curves of the Kilonova Associated with the Binary Neutron Star Merger GW170817: Unified Data Set, Analytic Models, and Physical Implications. *Astrophys. J. Lett.* **851**, L21 (2017).
[23] Drout, M. R. *et al.* Rapidly Evolving and Luminous Transients from Pan-STARRS1. *Astrophys. J.* **794**, 23 (2014).
[24] Kasliwal, M. M. *et al.* Spitzer mid-infrared detections of neutron star merger GW170817 suggests synthesis of the heaviest elements. *Mon. Not. R. Astron. Soc.* **510**, L7–L12 (2022).
[25] Wollaeger, R. T. *et al.* Impact of ejecta morphology and composition on the electromagnetic signatures of neutron star mergers. *Mon. Not. R. Astron. Soc.* **478**, 3298–3334 (2018).
[26] Mei, A. *et al.* Gigaelectronvolt emission from a compact binary merger. *Nature* **612**, 236–239 (2022).
[27] Gillanders, J. H., Sim, S. A., Smartt, S. J., Goriely, S. & Bauswein, A. Modelling the spectra of the kilonova AT2017gfo – II: Beyond the photospheric epochs. *arXiv e-prints* arXiv:2306.15055 (2023).
[28] Joshi, Y. N., Tauheed, A. & Davison, I. G. The analysis of the $5s^25p^2$, $5s5p^3$ $5s^25p5d$, and $5s^25p6s$ configurations of Te III. *Canadian Journal of Physics* **70**, 740 (1992).
[29] Hotokezaka, K., Beniamini, P. & Piran, T. Neutron star mergers as sites of r-process nucleosynthesis and short gamma-ray bursts. *International Journal of Modern Physics D* **27**, 1842005 (2018).
[30] Gillanders, J. H., Smartt, S. J., Sim, S. A., Bauswein, A. & Goriely, S. Modelling the spectra of the kilonova AT2017gfo - I. The photospheric epochs. *Mon. Not. R. Astron. Soc.* **515**, 631–651 (2022).
[31] Pognan, Q., Jerkstrand, A. & Grumer, J. On the validity of steady-state for nebular phase kilonovae. *Mon. Not. R. Astron. Soc.* **510**, 3806–3837 (2022).
[32] Hotokezaka, K., Tanaka, M., Kato, D. & Gaigalas, G. Tellurium emission line in kilonova AT 2017gfo. *arXiv e-prints* arXiv:2307.00988 (2023).
[33] Madonna, S. *et al.* Neutron-capture Elements in Planetary Nebulae: First Detections of Near-infrared [Te III] and [Br V] Emission Lines. *Astrophys. J. Lett.* **861**, L8 (2018).
[34] Watson, D. *et al.* Identification of strontium in the merger of two neutron stars. *Nature* **574**, 497–500 (2019).
[35] Hotokezaka, K., Tanaka, M., Kato, D. & Gaigalas, G. Tungsten versus Selenium as a potential source of kilonova nebular emission observed by Spitzer. *Mon. Not. R. Astron. Soc.* **515**, L89–L93 (2022).
[36] Fong, W.-f. *et al.* Short GRB Host Galaxies. I. Photometric and Spectroscopic

Catalogs, Host Associations, and Galactocentric Offsets. *Astrophys. J.* **940**, 56 (2022).

[37] O'Connor, B. *et al.* A deep survey of short GRB host galaxies over z 0-2: implications for offsets, redshifts, and environments. *Mon. Not. R. Astron. Soc.* **515**, 4890–4928 (2022).

[38] Grindlay, J., Portegies Zwart, S. & McMillan, S. Short gamma-ray bursts from binary neutron star mergers in globular clusters. *Nature Physics* **2**, 116–119 (2006).

[39] Burns, E. *et al.* GRB 221009A: The Boat. *Astrophys. J. Lett.* **946**, L31 (2023).

[40] Gehrels, N. *et al.* A new γ-ray burst classification scheme from GRB060614. *Nature* **444**, 1044–1046 (2006).

[41] Gal-Yam, A. *et al.* A novel explosive process is required for the γ-ray burst GRB 060614. *Nature* **444**, 1053–1055 (2006).

[42] MichałowskI, M. J. *et al.* The second-closest gamma-ray burst: sub-luminous GRB 111005A with no supernova in a super-solar metallicity environment. *Astron. Astrophys.* **616**, A169 (2018).

[43] Levan, A. J. *et al.* A long-duration gamma-ray burst of dynamical origin from the nucleus of an ancient galaxy. *Nature Astronomy* **7**, 976–985 (2023).

[44] Sarin, N., Lasky, P. D. & Nathan, R. S. Missed opportunities: GRB 211211A and the case for continual gravitational-wave coverage with a single observatory. *Mon. Not. R. Astron. Soc.* **518**, 5483–5489 (2023).

[45] Metzger, B. D., Quataert, E. & Thompson, T. A. Short-duration gamma-ray bursts with extended emission from protomagnetar spin-down. *Mon. Not. R. Astron. Soc.* **385**, 1455–1460 (2008).

[46] Rosswog, S. Fallback accretion in the aftermath of a compact binary merger. *Mon. Not. R. Astron. Soc.* **376**, L48–L51 (2007).

[47] Desai, D., Metzger, B. D. & Foucart, F. Imprints of r-process heating on fallback accretion: distinguishing black hole-neutron star from double neutron star mergers. *Mon. Not. R. Astron. Soc.* **485**, 4404–4412 (2019).

[48] Siegel, D. M., Barnes, J. & Metzger, B. D. Collapsars as a major source of r-process elements. *Nature* **569**, 241–244 (2019).

[49] Gottlieb, O. *et al.* Large-scale Evolution of Seconds-long Relativistic Jets from Black Hole-Neutron Star Mergers. *Astrophys. J. Lett.* **954**, L21 (2023).

[50] Gottlieb, O., Metzger, B. D., Quataert, E., Issa, D. & Foucart, F. A Unified Picture of Short and Long Gamma-ray Bursts from Compact Binary Mergers. *arXiv e-prints* arXiv:2309.00038 (2023).

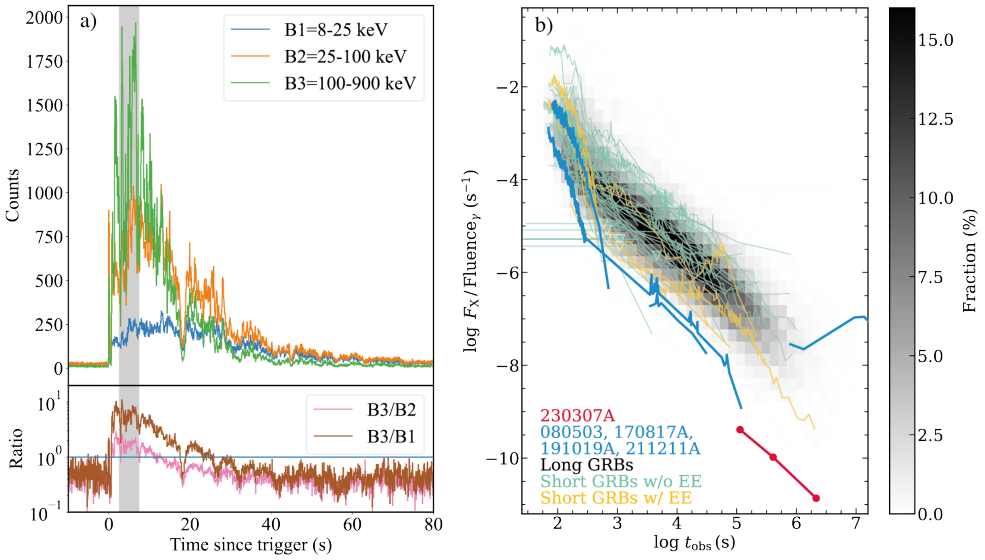

Fig. 1 The high energy properties of GRB 230307A. Panel a shows the light curve of the GRB at 64 ms time resolution with the *Fermi*/GBM. The shaded region indicates the region where saturation may be an issue. The burst begins very hard, with the count rate dominated by photons in the hardest (100-900 keV) band, but rapidly softens, with the count rate in the hard band being progressively overtaken by softer bands (e.g. 8-25 keV and 25-100 keV) beyond $\sim$ 20s. This strong hard-to-soft evolution is reminiscent of GRB 211211A [20] and is caused by the motion of two spectral breaks through the γ-ray regime (see Methods). Panel b shows the X-ray light curves of GRBs from the *Swift* X-ray telescope. These have been divided by the prompt fluence of the burst, which broadly scales with the X-ray light curve luminosity, resulting in a modest spread of afterglows. The greyscale background represents the ensemble of long GRBs. GRB 230307A is an extreme outlier of the $>$ 1000 *Swift*-GRBs, with an extremely faint afterglow for the brightness of its prompt emission. Other merger GRBs from long bursts occupy a similar region of parameter space. This suggests the prompt to afterglow fluence could be a valuable tool in distinguishing long GRBs from mergers and those from supernovae.

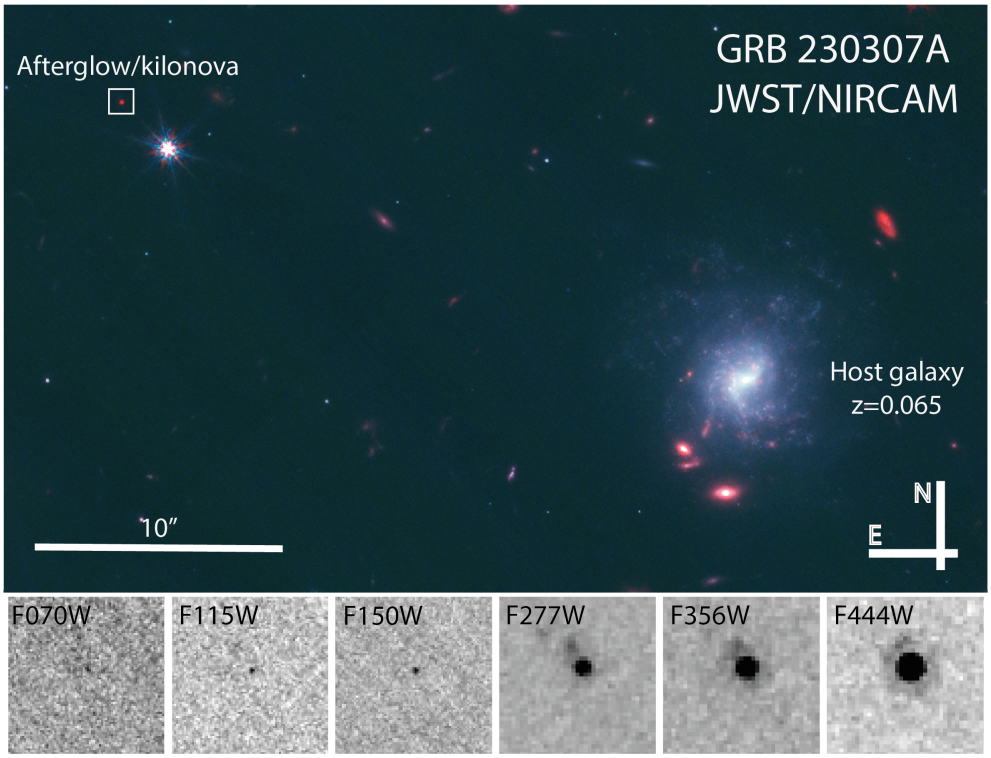

Fig. 2 JWST images of GRB 230307A at 28.5 days post burst. The upper region shows the wide field image combining the F115W, F150W and F444W images. The putative host is the bright face-on spiral galaxy, while the afterglow appears at a 30-arcsecond offset, within the white box. The lower panels shows cut-outs of the NIRCAM data around the GRB afterglow location. The source is faint and barely detected in the bluer bands but very bright and well detected in the red. In the red bands, a faint galaxy is present northeast of the transient position. This galaxy has a redshift of $z = 3.87$, but we consider it to be a background object unrelated to the GRB (see Supplementary Information).

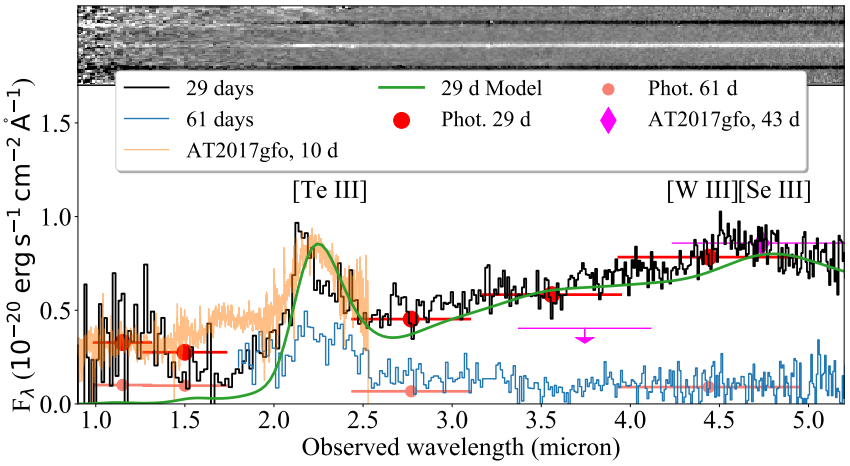

Fig. 3 JWST/NIRSpec spectroscopy of the counterpart of GRB 230307A. The top portion shows the 2-D spectrum rectified to a common wavelength scale. The transient is well detected beyond 2 microns but not short ward, indicative of an extremely red source. Emission lines from the nearby galaxy at $z = 3.87$ can also be seen offset from the afterglow trace. The lower panel shows the 1D extraction of the spectrum in comparison with the latest (10-day) AT2017gfo epoch and different kilonova models. A clear emission feature can be seen at ~ 2.15 microns at both 29 and 61 days. This feature is consistent with the expected location of [Te III], while redder features are compatible with lines from [Se III] and [W III]. This line is also clearly visible in the scaled late time spectrum of AT2017gfo [27, 32], while the red colours are also comparable to those of AT2017gfo as measured with *Spitzer* (show scaled to the 29 day NIRSpec spectrum). Error bars on photometry refer to the 1-σ error bar in this y-axis and the filter width on the x-axis.

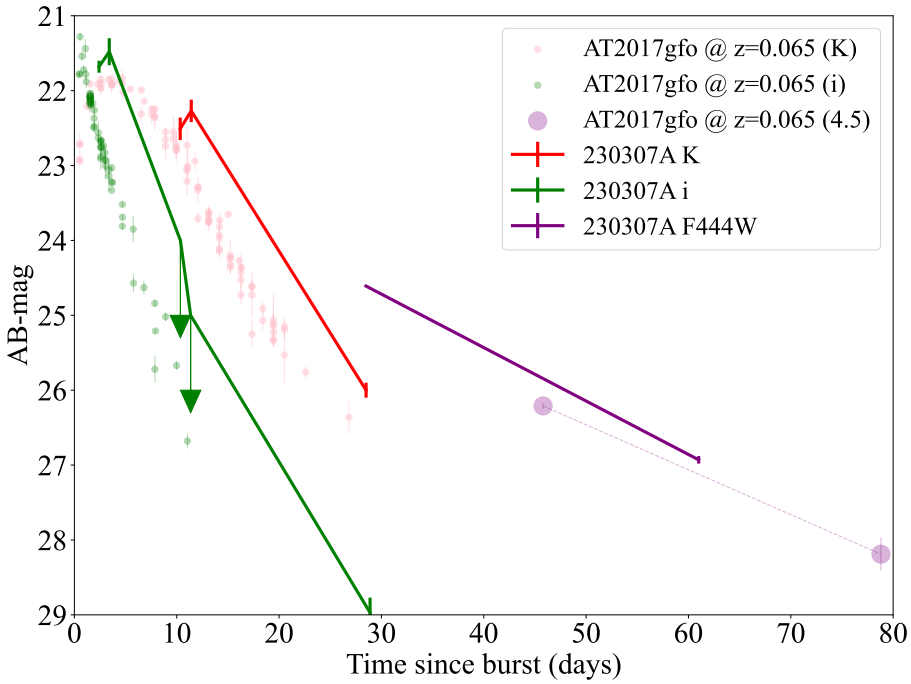

Fig. 4 A comparison of the counterpart of GRB 230307A with AT2017gfo associated with GW170817.AT2017gfo has been scaled to the same distance as GRB 230307A. Beyond ~ 2 days, the kilonova dominates the counterpart. The decay rates in both the optical and IR are very similar to those in AT2017gfo. These are too rapid for any plausible afterglow model. There is also good agreement in the late time slope between the measurements made at 4.4 microns with JWST and 4.5 microns for AT2017gfo with *Spitzer* [24]. Error bars refer to the 1σ uncertainty.

1 Methods

2 Observations

Below we outline the observational data that were used in this paper. Magnitudes are given in the AB system unless stated otherwise. We utilize cosmology resulting from the Planck observations [51]. All uncertainties are given at the 1σ level unless explicitly stated.

2.1 γ-ray observations

GRB 230307A was first detected by *Fermi*/GBM and GECAM at 15:44:06 UT on 7 Mar 2023 [13, 14]. It had a duration of $T_{90} \sim 35$s and an exceptionally bright prompt fluence of $(2.951 \pm 0.004) \times 10^{-3}\,\mathrm{erg\,cm^{-2}}$ [52]. The burst fell outside of the coded field-of-view of the *Swift* Burst Alert Telescope (BAT), and so did not receive a sub-degree localisation despite a strong detection. However, detections by *Swift*, GECAM [53], STIX on the Solar Orbiter [54], AGILE [55], ASTROSAT [56], GRBalpha [57], VZLUSAT [58], Konus-WIND [59] and ASO-HXI [60] enabled an enhanced position via the InterPlanetary Network to increasingly precise localisations of 1.948 deg^2 [61], 30 arcmin^2 [62], and ultimately to 8 arcmin^2 [15]. This was sufficiently small to enable tiling with *Swift* and ground-based telescopes.

2.1.1 *Fermi*/GBM data analysis

In Figure 1, we plot the light curve of GRB 230307A as seen by the *Fermi*/GBM in several bands, built by selecting Time Tagged Event (TTE) data, binned with a time resolution of 64 ms. The highlighted time interval of 3–7 s after trigger is affected by data loss due to the bandwidth limit for TTE data [63].

For the spectral analysis, we made use of the CSPEC data, which have 1024 ms time resolution. Data files were obtained from the online archive[1]. Following the suggestion reported by the *Fermi* Collaboration [63], we analysed the data detected by NaI 10 and BGO 1, which had a source viewing angle less than 60°, and excluded the time intervals affected by pulse pile-up issues (from 2.5 s to 7.5 s). The data extraction was performed with the public software GTBURST, while data were analysed with XSPEC. The background, whose time intervals have been selected before and after the source, was modelled with a polynomial function whose order is automatically found by GTBURST and manually checked. In the fitting procedure, we used inter–calibration factors among the detectors, scaled to the only NaI analysed and free to vary within 30%. We used the PG-Statistic, valid for Poisson data with a Gaussian background. The best-fit parameters and their uncertainties were estimated through a Markov Chain Monte Carlo (MCMC) approach. We selected the time intervals before and after the excluded period of 2.5-7.5 s due to instrumental effects. In particular, we extracted 2 time intervals from 0 to 2.5 s (1.25 s each) and 14 time intervals from 7.5 s to 40.5 (bin width of 2 s, except the last two with integration of 5 s to increase the signal-to-noise ratio), for a total of 16 time intervals. We fitted the corresponding

[1] https://heasarc.gsfc.nasa.gov/W3Browse/fermi/fermigbrst.html

spectra with the two smoothly broken power-law (2SBPL) function [64, 65], which has been shown to successfully model the synchrotron-like spectral shape of bright long GRBs, including the merger-driven GRB 211211A [20].

From our spectral analysis, we found that all spectra up to ~ 20 s are well modelled by the 2SBPL function, namely they are described by the presence of two spectral breaks inside the GBM band (8 keV–40 MeV). In particular, in the time intervals between 7.5 and 19.5 s, the low-energy break $E_{\rm break}$ is coherently decreasing from $304.3^{+5.2}_{-2.6}$ keV down to $52.1^{+4.3}_{-5.1}$ keV, and the typical νF_ν peak energy $E_{\rm peak}$ is also becoming softer, moving from $\sim$ 1 MeV to 450 keV. The spectral indices of the two power-laws below and above the low-energy break are distributed around the values of -0.82 and -1.72, which are similar to the predictions for synchrotron emission in marginally fast-cooling regime (i.e. $-2/3$ and $-3/2$). This is consistent with what has been found in GRB 211211A [20]. We notice, however, that in all spectra the high-energy power-law above $E_{\rm peak}$ is characterised by a much softer index (with a mean value of -4.10 ± 0.24) with respect to the value of $\sim$ -2.5 typically found in *Fermi* GRBs. This suggests that the spectral data might require a cut-off at high energy, although further investigations are needed to support this. From 19.5 s until 40.5 s (the last time interval analysed), all the break energies are found to be below 20 keV, close to the GBM low energy threshold. In the same time intervals, the peak energy $E_{\rm peak}$ decreases from $682.4^{+3.2}_{-6.1}$ to $123.1^{+5.4}_{-4.9}$ keV, and the index of the power-law below the peak energy is fully consistent (mean value of -1.45 ± 0.06) with the synchrotron predicted value of -1.5.

2.2 Optical observations

2.2.1 NTT - Afterglow discovery

Following the refinement of the IPN error box to an area of 30 arcmin^2 [62], we obtained observations of the field of GRB 230307A with the ULTRACAM instrument [66], mounted on the 3.5m New Technology Telescope (NTT) at La Silla, Chile. The instrument obtains images in 3 simultaneous bands, and is optimised for short exposure, low dead-time observations [66]. We obtained 10×20 s exposures in two pointings in each of the Super SDSS u, g and r, bands (where the Super SDSS bands match the wavelength range of the traditional SDSS filters but with a higher throughput; [67]). The observations began at 01:53:21 UT on 2023-03-09, approximately 34 hr after the GRB. The images were reduced via the HIPERCAM pipeline [67] using bias and flat frames taken on the same night. Visual inspection of the images compared to those obtained with the Legacy Survey [68] revealed a new source coincident with an X-ray source identified via *Swift*/XRT observations [16], and we identified it as the likely optical afterglow of GRB 230307A [17]. The best available optical position of this source (ultimately measured from our *JWST* observations, see below) is RA(J2000) = 04:03:26.02, Dec(J2000) = $-$75:22:42.76, with an uncertainty of 0.05 arcseconds in each axis (Supplementary Figure 1)

This identification was subsequently confirmed via observations from a number of additional observatories, including [69, 70, 71, 72, 73, 74]. We acquired two further

epochs of observations with ULTRACAM on the following nights with 10×20s exposures in the Super SDSS u, g and i, bands. Aperture photometry of the source is reported in Extended Data Table 1, and is reported relative to the Legacy survey for the gri bands, and to SkyMapper for the u-band.

2.2.2 TESS

The prompt and afterglow emission of GRB 230307A was detected by TESS, which observed the field continuously from 3 days before the *Fermi* trigger to 3 days after at a cadence of 200 s [75]. A reference image was subtracted from the observations to obtain GRB-only flux over this period. The measured flux in the broad TESS filter (600nm – 1000nm) is corrected for Galactic extinction and converted to the I_c band assuming a power-law spectrum with $F \propto \nu^{-0.8}$. We then bin the light curve logarithmically, taking the mean flux of the observations in each bin and converting to AB magnitudes. A systematic error of 0.1 magnitudes was added in quadrature to the measured statistical errors to account for the uncertainties in the data processing. These data are presented in Extended Data Table 1.

2.2.3 *Swift*/UVOT

The *Swift* Ultra-violet/Optical Telescope (UVOT [76]) began observing the field of GRB 230307A ~ 84.6 ks after the *Fermi*/GBM trigger [13]. The source counts were extracted using a source region of 5 arcsec radius. Background counts were extracted using a circular region of 20 arcsec radius located in a source-free part of the sky. The count rates were obtained from the image lists using the *Swift* tool UVOTSOURCE. A faint catalogued unrelated source also falls within the 5 arcsec radius, this will affect the photometry, particularly at late times. We, therefore, requested a deep template image in *white* in order to estimate the level of contamination. We extracted the count rate in the template image using the same 5 arcsec radii aperture. This was subtracted from the source count rates to obtain the afterglow count rates. The afterglow count rates were converted to magnitudes using the UVOT photometric zero points [77, 78].

2.2.4 Gemini

We obtained three epochs of K-band observations using the FLAMINGOS-2 instrument on the Gemini-South telescope. These observations were reduced through the DRAGONS pipeline to produce dark and sky-subtracted and flat-fielded images [79]. At the location of the optical counterpart to GRB 230307A, we identify a relatively bright K-band source in the first and second epochs, with only a upper limit in epoch 3. We report our photometry, performed relative to secondary standards in the VISTA hemisphere survey [80], in Extended Data Table 1.

2.2.5 VLT imaging

We carried out observations of the GRB 230307A field with the 8.2-m VLT telescopes located in Cerro Paranal, Chile. The observations were obtained with the FORS2 camera (mounted on the Unit Telescope 1, UT1, ANTU) in B, R, I and z bands at

multiple epochs, and with the HAWK-I instrument (mounted on the Unit Telescope 4, UT4, Yepun) in the K band at one epoch. All images were reduced using the standard ESO (European Southern Observatory) Reflex pipeline [81]. The source was detected in the FORS2 z-band image at ∼6.4 days after the *Fermi*/GBM detection. A single r'-band observation of the GRB 230307A was also executed with the 2.6m VLT Survey Telescope (VST) after 2.37 days from the GRB discovery. In later observations the source was not detected (see Supplementary Information) and the upper limit values at 3σ level are reported in Extended Data Table 1.

2.2.6 VLT spectroscopy

To attempt to measure the redshift of GRB 230307A and the nearby candidate host galaxies, we obtained spectroscopy with the VLT utilising both the X-shooter and MUSE instruments, mounted respectively on the Unit Telescope 3 (UT3, Melipal) and on UT4 (Yepun).

X-shooter spectroscopy, covering the wavelength range 3000–22000 Å was undertaken on 2023-03-15. Observations were taken at a fixed position angle, with the slit centred on a nearby bright star. X-shooter data have been reduced with standard *esorex* recipes. Given that only two of the four nod exposures were covering the GRB position, resulting in a total exposure time of 2400s on-source, we have reduced each single exposure using the stare mode data reduction. Then, we have stacked the two 2D frames covering the GRB position using dedicated post-processing tools developed in a python framework [82].

We further obtained observations with the MUSE integral field unit on 2023-03-23. The MUSE observations cover multiple galaxies within the field, as well as the GRB position, and cover the wavelength range 4750-9350 Å. MUSE data have been reduced using standard *esorex* recipes embedded within a single python script that performs the entire data reduction procedure. Later, the resulting datacube has been corrected for sky emission residuals using ZAP [83]. The MUSE observations reveal the redshifts for a large number of galaxies in the field, including a prominent spiral G1 at $z = 0.0646$ (see also [18]) and a group of galaxies, G2, G3 and G4 at $z = 0.263$, details are provided in Extended Data Table 3.

2.3 X-ray afterglow

Swift began tiled observations of the IPN localisation region with its X-ray Telescope [**?**, XRT;]]burrows05 at 12:56:42 on 8 Mar 2023[2] [84]. XRT made the first reported detection of the afterglow (initially identified as 'Source 2') with a count rate of $0.019 \pm 0.004\,\mathrm{cts}^{-1}$ [85] and later confirmed it to be fading with a temporal power-law index of $1.1^{+0.6}_{-0.5}$ [86]. XRT data were downloaded from the UK *Swift* Science Data Centre (UKSSDC [87, 88]).

We further obtained observations with the *Chandra* X-ray observatory (programme ID 402458: PI Fong/Gompertz). A total of 50.26 ks (49.67 ks of effective exposure) of data were obtained in three visits between 31 March 2023 and 2 April 2023. The source was placed at the default aim point on the S3 chip of the ACIS detector. At

[2] https://www.swift.ac.uk/xrt_products/TILED_GRB00110/

the location of the optical and X-ray afterglow of GRB 230307A, we detect a total of 12 counts, with an expected background of ~ 1, corresponding to a detection of the afterglow at $> 5\sigma$ based on the photon statistics of [89]. To obtain fluxes, we performed a joint spectral fit of the *Chandra* and *Swift*/XRT data. The best fitting spectrum, adopting uniform priors on all parameters, is a power law with a photon index of $\Gamma = 2.50^{+0.30}_{-0.29}$ when fitting with a Galactic $N_H = 1.26 \times 10^{21}$ cm^{-2} [90] and zero intrinsic absorption (neither XRT nor *Chandra* spectra have sufficient signal to noise to constrain any intrinsic absorption component). The resultant flux in the 0.3 – 10 keV band is $F_{\rm X}(1.7\,{\rm d}) = 4.91^{+0.89}_{-0.79} \times 10^{-13}$ erg cm^{-2} s^{-1} during the XRT observation and $F_{\rm X}(24.8\,{\rm d}) = 1.19^{+0.87}_{-0.62} \times 10^{-14}$ erg cm^{-2} s^{-1} during the Chandra observation. Due to the low count number, the *Chandra* flux posterior support extends to considerably below the reported median, with the 5th percentile being as low as $F_{\rm X,5th} = 3 \times 10^{-15}$ erg cm^{-2} s^{-1}. If a uniform-in-the-logarithm prior on the flux were adopted, this would extend to even lower values. *Chandra* and XRT fluxes are converted to 1 keV flux densities using the best fit spectrum (Extended Data Table 2)

2.4 ATCA

Following the identification of the optical afterglow [91], we requested target of opportunity observations of GRB 230307A (proposal identification CX529) with the Australia Telescope Compact Array (ATCA) to search for a radio counterpart. These data were processed using MIRIAD [92], which is the native reduction software package for ATCA data using standard techniques. Flux and bandpass calibration were performed using PKS 1934–638, with phase calibration using interleaved observations of 0454-810.

The first observation took place on 2023-03-12 at 4.46 d post-burst, which was conducted using the 4 cm dual receiver with frequencies centered at 5.5 and 9 GHz, each with a 2 GHz bandwidth. The array was in the 750C configuration[3] with a maximum baseline of 6 km. A radio source was detected at the position of the optical afterglow at 9 GHz with a flux density of $92 \pm 22\mu$Jy but went undetected at 5.5 GHz (3σ upper limit of 84μJy). A further two follow-up observations were also obtained swapping between the 4 cm and 15 mm dual receivers (the latter with central frequencies of 16.7 and 21.2 GHz, each with a 2 GHz bandwidth). During our second epoch at 10.66 d we detected the radio counterpart again, having become detectable at 5.5 GHz with marginal fading at 9 GHz. By the third epoch, the radio afterglow had faded below detectability. We did not detect the radio transient at 16.7 or 21.2 GHz in either epoch. All ATCA flux densities are listed in Extended Table 2.

2.5 MeerKAT

We were awarded time to observe the position of GRB 230307A with the MeerKAT radio telescope via a successful Directors Discretionary Time proposal (PI: Rhodes, DDT-20230313-LR-01). The MeerKAT radio telescope is a 64-dish interferometer based in the Karoo Desert, Northern Cape, South Africa [93]. Each dish is 12 m in diameter and the longest baseline is $\sim$8 km allowing for an angular resolution of

[3] https://www.narrabri.atnf.csiro.au/operations/array_configurations/configurations.html

~ 7 arcsec and a field of view of 1 deg^2. The observations we were awarded were made at both L and S-band.

GRB 230307A was observed over three separate epochs between seven and 41 days post-burst. The first two observations were made at both L and S4-band (the highest frequency of the five S-band sub-bands), centred at 1.28 and 3.06 GHz with a bandwidth of 0.856 and 0.875 GHz, respectively. Each observation spent two hours at L-band and 20 minutes at S4-band. The final observation was made only at S4-band with one hour on target. Please see the paper by MPIfR for further details on the new MeerKAT S-band receiver.

Each observation was processed using OXKAT, a series of semi-automated Python scripts designed specifically to deal with MeerKAT imaging data [94]. The scripts average the data and perform flagging on the calibrators from which delay, bandpass and gain corrections are calculated and then applied to the target. The sources J0408-6545 and J0252-7104 were used at the flux and complex gain calibrator, respectively. Flagging and imaging of the target field are performed. We also perform a single round of phase-only self-calibration. We do not detect a radio counterpart in any epoch in either band. The RMS noise in the field was measured using an empty region of the sky and used to calculate 3σ upper limits which are given in Extended Data Table 2.

2.6 JWST observations

We obtained two epochs of observations of the location of GRB 230307A with JWST. The first on 5 April 2023, with observations beginning at 00:16 UT (MJD=60039.01), 28.4 days after the burst (under programme GO 4434, PI Levan), and the second on 8 May 2023, 61.5 days after the burst (programme 4445, PI Levan). The observations were at a post-peak epoch because the source was not in the JWST field of regard at the time of the burst and only entered it on 2 April 2023.

At the first epoch, we obtained observations in the F070W, F115W, F150W, F277W, F356W and F444W filters of NIRCam [95], as well as a prism spectrum with NIRSpec [96]. In the second epoch we obtained NIRCam observations in F115W, F150W, F277W and F444W and a further NIRSpec prism observation. However, in the second epoch the prism observation is contaminated by light from the diffraction spike of a nearby star and is of limited use, in particular at the blue end of the spectrum. We therefore use only light redward of 1.8 microns. However, even here we should be cautious in interpreting the overall spectral shape. The feature at 2.15 microns is visible in both the 29 and 61 day spectra.

We reprocessed and re-drizzled the NIRCam data products to remove $1/f$ striping and aid point spread function recovery, with the final images having plate scales of 0.02 arcsec/pixel (blue channel) and 0.04 arcsec/pixel (red channel).

In the NIRCam imaging we detect a source at the location of the optical counterpart of GRB 230307A. This source is weakly detected in all three bluer filters (F070W, F115W and F150W), but is at high signal-to-noise ratio in the redder channels (see Figure 2). The source is compact and unresolved. We also identify a second source offset (H1) approximately 0.3 arcsec from the burst location. This source is also weakly, or non-detected in the bluer bands, and is brightest in the F277W filter.

Because of the proximity of the nearby star and a contribution from diffraction spikes close to the afterglow position we model point spread functions for the appropriate bands using WebbPSF [97], and then scale and subtract these from star position. Photometry is measured in small (0.05 arcsec (blue) and 0.1 arcsec (red)) apertures and then corrected using tabulated encircled energy corrections. In addition to the direct photometry of the NIRCam images we also report a a K-band point based on folding the NIRSpec spectrum (see below), through a 2MASS, Ks filter. This both provides a better broadband SED and a direct comparison with ground based K-band observations. Details of photometric measurements are shown in Extended Data Table 1

For NIRSpec, we utilise the available archive-processed level 3 two-dimensional spectrum (Figure 3). In this spectrum we clearly identify the trace of the optical counterpart, which appears effectively undetected until 2 microns and then rises rapidly. We also identify two likely emission lines which are offset from the burst position. These are consistent with the identification with Hα and [O III] (4959/5007) at a redshift of $z = 3.87$. Both of these lines lie within the F277W filter in NIRCam and support the identification of the nearby source as the origin of these lines.

We extract the spectrum in two small (2 pixel) apertures. One of these is centred on the transient position, while the second is centred on the location of the emission lines. Since the offset between these two locations is only ~ 0.3 arcsec there is naturally some contamination of each spectrum with light from both sources, but this is minimised by the use of small extraction apertures. The resulting 1D spectra are shown in Figure 3. The counterpart is very red, with a sharp break at 2 microns and an apparent emission feature at 2.15 microns. The spectrum then continues to rise to a possible second feature (or a change in the associated spectral slope) at around 4.5 microns.

Author contribution statements

AJL led the project, including the location of the optical afterglow and kilonova and the JWST observations. BPG first identified the source as a likely compact object merger, was co-PI of the *Chandra* observations, and contributed to analysis and writing. OSS contributed to afterglow and kilonova modelling and led the writing of these sections. MB was involved in kilonova modelling, EB contributed to interpretation, placing the burst in context and high energy properties. KH was involved in kilonova spectral modelling and identified the 2.15 μm feature. LI contributed to the X-shooter data analysis, reduced the MUSE data, and led the host analysis. GPL contributed to afterglow and kilonova modelling. DBM organized the VLT observations and contributed to the data analysis. MER analyzed the *Fermi* data. ARE analysed the Chandra observations, BS reduced and analysed VLT observations. NS contributed to afterglow and kilonova modelling. SS was responsible for placing the burst afterglow in context and demonstrating its faintness. NRT contributed to observations and interpretation. KA was involved in the ULTRACAM observations. GA led the ATCA observations. GB reduced the JWST NIRCam data. LC processed and analysed the MUSE observations. VSD is the ULTRACAM PI. JPUF studied the high-z possibilities. WF was the PI on the Chandra observations. CF contributed to the theoretical interpretation. NG was involved in host analysis. JTP contributed to the JWST spectrum visualisation. KEH, GP, AR, SDV, SC, PDA, DH, MDP, CCT, AdUP and DA contributed to ESO observations and discussion. DW contributed to spectral and progenitor modelling. MJD, PK, SP, JM, SGP, IP, DIS contributed to the ULTRACAM observations. AS reduced X-shooter observations. GL investigated potential similarities with other transients. AT, PAE, BS and JAK contributed to the *Swift* observations. MF extracted and flux-calibrated the TESS light curve. SJS analysed the JWST spectral lines. HFS performed the BPASS-hoki-ppxf fits to the integrated MUSE flux and contributed the associate figure and text. All authors contributed to manuscript preparation through contributions to concept development, discussion and text.

Acknowledgements

We dedicate this paper to David Alexander Kann, who passed on March 10. He was the first to realise the exceptional brightness of GRB 230307A, and the final messages he sent were regarding its follow-up. We hope it would satisfy his curiosity to know the final conclusions.

This work is based on observations made with the NASA/ESA/CSA James Webb Space Telescope. The data were obtained from the Mikulski Archive for Space Telescopes at the Space Telescope Science Institute, which is operated by the Association of Universities for Research in Astronomy, Inc., under NASA contract NAS 5-03127 for JWST. These observations are associated with program #4434 and 4445. Support for Program numbers 4434 and 4445 was provided through grants from the STScI under NASA contract NAS5- 03127.

This paper is partly based on observations collected at the European Southern Observatory under ESO programme 110.24CF (PI Tanvir), and on observations obtained at the international Gemini Observatory (program ID GS-2023A-DD-105),

a program of NOIRLab, which is managed by the Association of Universities for Research in Astronomy (AURA) under a cooperative agreement with the National Science Foundation on behalf of the Gemini Observatory partnership: the National Science Foundation (United States), National Research Council (Canada), Agencia Nacional de Investigación y Desarrollo (Chile), Ministerio de Ciencia, Tecnología e Innovación (Argentina), Ministério da Ciência, Tecnologia, Inovações e Comunicações (Brazil), and Korea Astronomy and Space Science Institute (Republic of Korea). Processed using the Gemini `IRAF` package and `DRAGONS` (Data Reduction for Astronomy from Gemini Observatory North and South).

AJL, DBM and NRT were supported by the European Research Council (ERC) under the European Unions Horizon 2020 research and innovation programme (grant agreement No. 725246). MB acknowledges the Department of Physics and Earth Science of the University of Ferrara for the financial support through the FIRD 2022 grant. KH is supported by JST FOREST Program (JPMJFR2136) and the JSPS Grant-in-Aid for Scientific Research (20H05639, 20H00158, 23H01169, 20K14513). GPL is supported by a Royal Society Dorothy Hodgkin Fellowship (grant Nos. DHF-R1-221175 and DHF-ERE-221005). MER acknowledges support from the research programme Athena with project number 184.034.002, which is financed by the Dutch Research Council (NWO). NS is supported by a Nordita fellowship. Nordita is supported in part by NordForsk. SS acknowledges support from the G.R.E.A.T. research environment, funded by *Vetenskapsrådet*, the Swedish Research Council, project number 2016-06012. VSD and ULTRACAM are funded by STFC grant ST/V000853/1. GL was supported by a research grant (19054) from VILLUM FONDEN. The Cosmic Dawn Center (DAWN) is funded by the Danish National Research Foundation under grant No. 140. JPUF is supported by the Independent Research Fund Denmark (DFF4090-00079) and thanks the Carlsberg Foundation for support. DW is co-funded by the European Union (ERC, HEAVYMETAL, 101071865). DKG acknowledges support from the Australian Research Council Centre of Excellence for Gravitational Wave Discovery (OzGrav), through project number CE170100004. NG acknowledges support from the Dutch Research Council (NWO) under the project number 680.92.18.02. KEH acknowledges support from the Carlsberg Foundation Reintegration Fellowship Grant CF21-0103. JH and DL were supported by a VILLUM FONDEN Investigator grant (project number 16599). BDM is supported in part by the NSF (grant AST-2002577). MN is supported by the European Research Council (ERC) under the European Unions Horizon 2020 research and innovation programme (grant agreement No. 948381) and by UK Space Agency Grant No. ST/Y000692/1. SJS acknowledges funding from STFC Grant ST/X006506/1 and ST/T000198/1. H.F.S is supported by the Eric and Wendy Schmidt AI in Science Postdoctoral Fellowship, a Schmidt Futures program. AAB acknowledges funding from the UK Space Agency. POB acknowledges funding from STFC grant ST/W000857/1. DS acknowledges funding from STFC grants ST/T000406/1, ST/T003103/1, ST/X001121/1. AS acknowledges support from DIM-ACAV+ and CNES. SC, PDA, BS and GT acknowledge funding from the Italian Space Agency, contract ASI/INAF n. I/004/11/4.

Data availability

JWST data are directly available from the MAST archive archive.stsci.edu. ESO data can be obtained from archive.eso.org and Gemini data from archive.gemini.edu. Core reduced optical and IR products can also be downloaded directly from the Electronic Research Data Archive at the University of Copenhagen (ERDA) via https://sid.erda.dk/sharelink/b35FULIcV5. This research has made use of *Fermi* data which are publicly available and can be obtained through the High Energy Astrophysics Science Archive Research Center (HEASARC) website at https://heasarc.gsfc.nasa.gov/W3Browse/fermi/fermigbrst.html. *Swift* data can be obtained from http://www.swift.ac.uk/xrt_curves and *Chandra* observations from https://cda.harvard.edu/chaser/

Code availability

Much analysis for this paper has been undertaken with publicly available codes and the details required to reproduce the analysis are contained within the manuscript.

Competing Intrests

The authors confirm they have no competing interests.

3 Extended Data

Extended data table 1 caption: Optical and IR observations of the optical counterpart of GRB 230307A. Errors are given at 1σ, and limits are given at the 3σ level.

Extended data table 2 caption: X-ray and radio observations of the afterglow of GRB 230307A. Errors are given at the 1σ level and upper limits at the 3σ level.

Extended data table 3 caption: Properties of possible host galaxies for GRB 230307A. *Formally, because the galaxy is undetected in the $r-$band, P_{chance} is unbounded. This probability is based on the magnitudes measured at other wavelengths.

Time since GRB (days)	Telescope	Band	Exposure time (s)	Magnitude (AB)	Source
0.01	TESS	I_C	1600	18.63 ± 0.14	This work
0.03	TESS	I_C	1600	18.15 ± 0.12	This work
0.04	TESS	I_C	1600	17.98 ± 0.11	This work
0.09	TESS	I_C	6400	18.06 ± 0.10	This work
0.19	TESS	I_C	11200	18.41 ± 0.10	This work
0.38	TESS	I_C	20800	19.23 ± 0.11	This work
0.64	TESS	I_C	24000	19.61 ± 0.16	This work
0.99	UVOT	U	2315	> 21.1	This work
1.16	UVOT	White	692	$22.25^{+0.23}_{-0.19}$	This work
1.25	UVOT	White	2217	$22.29^{+0.34}_{-0.26}$	This work
1.43	ULTRACAM	u	200	> 19.7	This work
1.43	ULTRACAM	g	200	> 20.7	This work
1.43	ULTRACAM	r	200	20.72 ± 0.15	This work
1.61	UVOT	White	6468	> 22.60	This work
2.37	VST	r	360	21.84 ± 0.19	This work
2.41	ULTRACAM	u	200	> 21.2	This work
2.41	ULTRACAM	g	200	22.35 ± 0.26	This work
2.41	ULTRACAM	i	200	21.68 ± 0.09	This work
2.43	UVOT	White	3303	> 22.0	This work
3.39	ULTRACAM	u	200	> 20.8	This work
3.39	ULTRACAM	g	200	> 22.6	This work
3.39	ULTRACAM	i	200	21.48 ± 0.18	This work
4.89	UVOT	White	14921	> 23.6	This work
6.42	FORS2	z	1440	23.24 ± 0.11	This work
6.42	FORS2	B	1380	> 26.10	This work
10.34	FLAMINGOS-2	K	840	22.51 ± 0.15	This work
10.36	FORS2	I	2400	> 24.0	This work
11.36	FORS2	I	2400	> 25.2	This work
11.42	FLAMINGOS-2	K	700	22.27 ± 0.15	This work
15.45	FLAMINGOS-2	K	950	> 22.1	This work
17.38	FORS2	R	3000	> 25.2	This work
19.37	FORS2	R	3000	> 25.8	This work
19.38	HAWK-I	K	2340	> 23.4	This work
28.89	JWST	F070W	1868	28.97 ± 0.20	This work
28.83	JWST	F115W	1868	28.50 ± 0.07	This work
28.86	JWST	F150W	1546	28.11 ± 0.12	This work
28.83	JWST	F277W	1868	26.24 ± 0.01	This work
28.86	JWST	F356W	1546	25.42 ± 0.01	This work
28.89	JWST	F444W	1868	24.62 ± 0.01	This work
61.48	JWST	F115W	1868	29.78 ± 0.31	This work
61.51	JWST	F150W	1546	29.24 ± 0.17	This work
61.51	JWST	F277W	1868	28.31 ± 0.12	This work
61.48	JWST	F444W	1546	26.97 ± 0.04	This work
2.35	GMOS-S	r	30	22.0 ± 0.3	[70]
2.35	SOAR	z	310	21.8 ± 0.3	[72]
3.35	SOAR	z	600	21.8 ± 0.3	[72]

Time since trigger (days)	Telescope	Frequency (Hz)	Flux density (μJy)	Source
1.7	*Swift*/XRT	2.42×10^{17}	$(6.5 \pm 1.1) \times 10^{-2}$	This work
9.59	*Swift*/XRT	2.42×10^{17}	$< 7.14 \times 10^{-3}$	[86]
24.84	*Chandra*	2.42×10^{17}	$1.6^{+1.2}_{-0.8} \times 10^{-3}$	This work
4.46	ATCA	5.5×10^{9}	< 84	This work
4.46	ATCA	9×10^{9}	92 ± 22	This work
10.66	ATCA	16.7×10^{9}	< 114	This work
10.66	ATCA	21.2×10^{9}	< 165	This work
10.69	ATCA	5.5×10^{9}	92 ± 36	This work
10.69	ATCA	9×10^{9}	83 ± 26	This work
25.55	ATCA	16.7×10^{9}	< 81	This work
25.55	ATCA	21.2×10^{9}	< 219	This work
25.59	ATCA	5.5×10^{9}	< 63	This work
25.59	ATCA	9×10^{9}	< 63	This work
6.64	MeerKAT	1.3×10^{9}	< 390	This work
6.75	MeerKAT	3.1×10^{9}	< 140	This work
15.74	MeerKAT	1.3×10^{9}	< 350	This work
16.04	MeerKAT	3.1×10^{9}	< 120	This work
40.89	MeerKAT	3.1×10^{9}	< 93	This work

Host candidate	RA	Dec	r	z	offset ($''$)	P_{chance}
H1	04:03:26.06	-75:22:42.5	> 29	3.87	0.30	0.05*
G1	04:03:18.79	-75:22:55.0	17.6	0.0645	29.9	0.09
G2	04:03:27.32	-75:23.09.3	18.6	0.2633	27.0	0.15
G3	04:03:25.64	-75:23:17.0	18.8	0.2626	34.2	0.27
G4	04:03:16.67	-75:22:23.2	19.4	0.2627	29.9	0.32

References

[51] Planck Collaboration *et al.* Planck 2018 results. VI. Cosmological parameters. *Astron. Astrophys.* **641**, A6 (2020).

[52] Dalessi, S., Roberts, O. J., Meegan, C. & Fermi GBM Team. GRB 230307A: Fermi GBM Observation of a very bright burst. *GRB Coordinates Network* **33411**, 1 (2023).

[53] Xiong, S., Wang, C., Huang, Y. & Gecam Team. GRB 230307A: GECAM detection of an extremely bright burst. *GRB Coordinates Network* **33406**, 1 (2023).

[54] Xiao, H. & Krucker, S. Solar Orbiter STIX observation of GRB 230307A. *GRB Coordinates Network* **33410**, 1 (2023).

[55] Casentini, C. *et al.* GRB 230307A: AGILE/MCAL detection. *GRB Coordinates Network* **33412**, 1 (2023).

[56] Navaneeth, P. K. *et al.* GRB 230307A: AstroSat CZTI detection. *GRB Coordinates Network* **33415**, 1 (2023).

[57] Dafcikova, M. *et al.* GRB 230307A: Detection by GRBAlpha. *GRB Coordinates Network* **33418**, 1 (2023).

[58] Ripa, J. *et al.* GRB 230307A: VZLUSAT-2 detection. *GRB Coordinates Network* **33424**, 1 (2023).

[59] Svinkin, D. *et al.* Konus-Wind detection of GRB 230307A. *GRB Coordinates Network* **33427**, 1 (2023).

[60] Li, Z., Su, Y. & HXI Team. GRB 230307A: ASO-S/HXI detection. *GRB Coordinates Network* **33438**, 1 (2023).

[61] Kozyrev, A. S. *et al.* IPN triangulation of GRB 230307A (long/very bright). *GRB Coordinates Network* **33413**, 1 (2023).

[62] Kozyrev, A. S. *et al.* Improved IPN localization for GRB 230307A. *GRB Coordinates Network* **33425**, 1 (2023).

[63] Dalessi, S. & Fermi GBM Team. GRB 230307A: Bad Time Intervals for Fermi GBM data. *GRB Coordinates Network* **33551**, 1 (2023).

[64] Ravasio, M. E. *et al.* Consistency with synchrotron emission in the bright GRB 160625B observed by Fermi. *Astron. Astrophys.* **613**, A16 (2018).

[65] Ravasio, M. E., Ghirlanda, G., Nava, L. & Ghisellini, G. Evidence of two spectral breaks in the prompt emission of gamma-ray bursts. *Astron. Astrophys.* **625**, A60 (2019).

[66] Dhillon, V. S. *et al.* ULTRACAM: an ultrafast, triple-beam CCD camera for high-speed astrophysics. *Mon. Not. R. Astron. Soc.* **378**, 825–840 (2007).

[67] Dhillon, V. S. *et al.* HiPERCAM: a quintuple-beam, high-speed optical imager on

the 10.4-m Gran Telescopio Canarias. *Mon. Not. R. Astron. Soc.* **507**, 350–366 (2021).
[68] Dey, A. *et al.* Overview of the DESI Legacy Imaging Surveys. *Astron. J.* **157**, 168 (2019).
[69] Lipunov, V. *et al.* GRB 230204B: MASTER detection of an object near NTT Optical Afterglow Candidate. *GRB Coordinates Network* **33441**, 1 (2023).
[70] O'Connor, B. *et al.* GRB 230307A: Gemini-South Confirmation of the Optical Afterglow. *GRB Coordinates Network* **33447**, 1 (2023).
[71] Im, M. *et al.* GRB 230307A: GECKO optical observations and detections of the afterglow. *GRB Coordinates Network* **33449**, 1 (2023).
[72] Bom, C. R. *et al.* GRB 230307A: SOAR/Goodman detection of the possible host galaxy. *GRB Coordinates Network* **33459**, 1 (2023).
[73] Breeveld, A. A., Salvaggio, C. & Swift/UVOT Team. GRB 230307A: Swift/UVOT detection. *GRB Coordinates Network* **33471**, 1 (2023).
[74] Gillanders, J., O'Connor, B., Dichiara, S. & Troja, E. GRB 230307A: Continued Gemini-South observations confirm rapid optical fading. *GRB Coordinates Network* **33485**, 1 (2023).
[75] Fausnaugh, M. M. *et al.* Observations of GRB 230307A by TESS. *Research Notes of the American Astronomical Society* **7**, 56 (2023).
[76] Roming, P. W. A. *et al.* The Swift Ultra-Violet/Optical Telescope. *Space Science Reviews* **120**, 95–142 (2005).
[77] Poole, T. S. *et al.* Photometric calibration of the Swift ultraviolet/optical telescope. *Mon. Not. R. Astron. Soc.* **383**, 627–645 (2008).
[78] Breeveld, A. A. *et al.* J. E. McEnery, J. L. Racusin, & N. Gehrels (ed.) *An Updated Ultraviolet Calibration for the Swift/UVOT.* (ed.J. E. McEnery, J. L. Racusin, & N. Gehrels) *American Institute of Physics Conference Series*, Vol. 1358 of *American Institute of Physics Conference Series*, 373–376 (2011). 1102.4717.
[79] Labrie, K., Anderson, K., Cárdenes, R., Simpson, C. & Turner, J. E. H. Teuben, P. J., Pound, M. W., Thomas, B. A. & Warner, E. M. (eds) *DRAGONS - Data Reduction for Astronomy from Gemini Observatory North and South.* (eds Teuben, P. J., Pound, M. W., Thomas, B. A. & Warner, E. M.) *Astronomical Data Analysis Software and Systems XXVII*, Vol. 523 of *Astronomical Society of the Pacific Conference Series*, 321 (2019).
[80] McMahon, R. G. *et al.* First Scientific Results from the VISTA Hemisphere Survey (VHS). *The Messenger* **154**, 35–37 (2013).
[81] Freudling, W. *et al.* Automated data reduction workflows for astronomy. The ESO Reflex environment. *Astron. Astrophys.* **559**, A96 (2013).
[82] Selsing, J. *et al.* The X-shooter GRB afterglow legacy sample (XS-GRB). *Astron. Astrophys.* **623**, A92 (2019).
[83] Soto, K. T., Lilly, S. J., Bacon, R., Richard, J. & Conseil, S. ZAP - enhanced PCA sky subtraction for integral field spectroscopy. *Mon. Not. R. Astron. Soc.* **458**, 3210–3220 (2016).
[84] Evans, P. A. & Swift Team. GRB 230307A: Tiled Swift observations. *GRB Coordinates Network* **33419**, 1 (2023).
[85] Burrows, D. N. *et al.* GRB 230307A: Swift-XRT observations. *GRB Coordinates*

Network **33429**, 1 (2023).

[86] Burrows, D. N. *et al.* Grb 230307a: Swift-xrt afterglow detection. *GRB Coordinates Network* **33465**, 1 (2023).

[87] Evans, P. A. *et al.* An online repository of Swift/XRT light curves of γ-ray bursts. *Astron. Astrophys.* **469**, 379–385 (2007).

[88] Evans, P. A. *et al.* Methods and results of an automatic analysis of a complete sample of Swift-XRT observations of GRBs. *Mon. Not. R. Astron. Soc.* **397**, 1177–1201 (2009).

[89] Kraft, R. P., Burrows, D. N. & Nousek, J. A. Determination of Confidence Limits for Experiments with Low Numbers of Counts. *Astrophys. J.* **374**, 344 (1991).

[90] Willingale, R., Starling, R. L. C., Beardmore, A. P., Tanvir, N. R. & O'Brien, P. T. Calibration of X-ray absorption in our Galaxy. *Mon. Not. R. Astron. Soc.* **431**, 394–404 (2013).

[91] Levan, A. J. *et al.* The First JWST Spectrum of a GRB Afterglow: No Bright Supernova in Observations of the Brightest GRB of all Time, GRB 221009A. *Astrophys. J. Lett.* **946**, L28 (2023).

[92] Sault, R. J., Teuben, P. J. & Wright, M. C. H. Shaw, R. A., Payne, H. E. & Hayes, J. J. E. (eds) *A Retrospective View of MIRIAD.* (eds Shaw, R. A., Payne, H. E. & Hayes, J. J. E.) *Astronomical Data Analysis Software and Systems IV*, Vol. 77 of *Astronomical Society of the Pacific Conference Series*, 433 (1995).

[93] Jonas, J. & MeerKAT Team. *The MeerKAT Radio Telescope*, 1 (2016).

[94] Heywood, I. oxkat: Semi-automated imaging of MeerKAT observations. Astrophysics Source Code Library, record ascl:2009.003 (2020). 2009.003.

[95] Beichman, C. A. *et al.* Clampin, M. C., Fazio, G. G., MacEwen, H. A. & Oschmann, J., Jacobus M. (eds) *Science opportunities with the near-IR camera (NIRCam) on the James Webb Space Telescope (JWST).* (eds Clampin, M. C., Fazio, G. G., MacEwen, H. A. & Oschmann, J., Jacobus M.) *Space Telescopes and Instrumentation 2012: Optical, Infrared, and Millimeter Wave*, Vol. 8442 of *Society of Photo-Optical Instrumentation Engineers (SPIE) Conference Series*, 84422N (2012).

[96] Jakobsen, P. *et al.* The Near-Infrared Spectrograph (NIRSpec) on the James Webb Space Telescope. I. Overview of the instrument and its capabilities. *Astron. Astrophys.* **661**, A80 (2022).

[97] Perrin, M. D. *et al.* Oschmann, J., Jacobus M., Clampin, M., Fazio, G. G. & MacEwen, H. A. (eds) *Updated point spread function simulations for JWST with WebbPSF.* (eds Oschmann, J., Jacobus M., Clampin, M., Fazio, G. G. & MacEwen, H. A.) *Space Telescopes and Instrumentation 2014: Optical, Infrared, and Millimeter Wave*, Vol. 9143 of *Society of Photo-Optical Instrumentation Engineers (SPIE) Conference Series*, 91433X (2014).